Plastic-Based Distributed Feedback Laser Biosensors in Microplate Format

Yafang Tan, Chun Ge, Allen Chu, Meng Lu, William Goldshlag, Jason Huang,

Anusha Pokriyal, Sherine George, Brian T. Cunningham, *Senior Member, IEEE*

***Abstract*—A process that combines polymer nanoreplica molding with horizontal dipping was used to fabricate large area (~3x5 inch^2) distributed feedback laser biosensors (DFBLB) on flexible plastic substrates, which were subsequently incorporated into standard format 96-well microplates. A room temperature nanoreplica molding process was used to create subwavelength periodic grating structures, while a horizontal dipping process was used to apply a ~300 nm, dye-doped polymer film. In this work, the DFBLB emission wavelength, used to characterize the device uniformity, demonstrated a coefficient of variation (CV) of 0.41% over the fabricated device area, representing a thickness standard deviation of only ~35 nm for the horizontal dipping process. The fabricated sensors were further characterized for sensitivity uniformity by measuring the bulk refractive index of the media exposed to the sensor surface and by measuring adsorption of biomolecular layers. An assay for detection of the cytokine Tumor Necrosis Factor-alpha (TNF-α) was used to demonstrate the operation of the sensor in the context of label-free detection of a disease biomarker. The demonstrated capability represents an important step towards roll-to-roll manufacturability for this biosensor that simultaneously incorporates high sensitivity with excellent wavelength shift resolution, and adaptability to the microplate format that is ubiquitous in pharmaceutical research.**

***Index Terms*—Horizontal dipping, label-free, distributed feedback laser biosensor, microplate format.**

I. Introduction

THERE is a continuing need to develop label-free detection methods that combine high sensitivity with high resolution for applications that include detection of low molecular weight analytes that bind to immobilized proteins, and the detection of protein analytes such as disease biomarkers that are present at low concentrations. While biosensors based upon optical resonators such as Surface Plasmon Resonance (SPR) [1-3] and Photonic Crystal (PC) surfaces [4, 5] have been commercially available for several years, and demonstrated for a wide range of applications, there has been a strong effort to improve upon their resolution performance through the implementation of resonators with more narrow resonant bandwidths (higher quality factor, as defined by $Q=\lambda_0/\Delta\lambda_0$). Whispering Gallery Mode (WGM) resonators such as microrings [6-8], liquid-core optical rings [9, 10], microspheres [11-13] and microtoroids [14, 15] are representative examples of passive high-Q resonators that have been implemented as biosensors. However, greater Q-factor is generally accompanied by reduced sensitivity, as measured by the magnitude of the wavelength shift obtained for adsorption of biomolecules. Furthermore, high Q-factor results in increased stringency for coupling light into the resonator, leading to a requirement for a precisely tunable wavelength excitation source that diminishes the applicability of high Q-factor resonators for high throughput measurements [16].

To be useful for applications in pharmaceutical high throughput screening (HTS), a biosensor technology must combine excellent uniformity, low-cost fabrication, compatibility with automated liquid handling equipment, (for example, through incorporation into standard format microplates), robust detection instrumentation, and the ability to rapidly measure many sensors. Sensor uniformity is a key requirement for life science applications because replicate measurements are used to determine the standard deviation and coefficient of variance of assays, which in turn determines the statistical relevance of the data. Furthermore, sensor-to-sensor uniformity is of equal importance to sensitivity in the determination of the Z-factor statistic [17] used to quantify the statistical quality of HTS data.

Recently, we have demonstrated a DFBLB that represents a departure from previous optical biosensor approaches based upon passive resonators [18, 19]. The DFBLB is an active device that achieves high Q-factor through the process of stimulated emission, resulting in Q in the range $1x10^4$ to $2x10^5$ without a reduction in wavelength shift sensitivity. The DFB cavity is based on a second-order Bragg grating that supports a

Manuscript received April 7, 2011. This work was supported in part by the National Institutes of Health (Grant R21 EB009695 A), the National Science Foundation (Grant ECCS 09-24062) and the Telemedicine & Advanced Technology Research Center (TATRC), under Contract W81XWH0810701.

Yafang Tan, Chun Ge, Allen Chu, William Goldshlag, Jason Huang and B. T. Cunningham are with the Department of Electrical and Computer Engineering, University of Illinois at Urbana–Champaign, Urbana, IL 61801 USA(e-mail: tan50@illinois.edu, chunge1@illinois.edu, chu32@illinois.edu, williamg@illinois.edu, csh@illinois.edu, bcunning@illinois.edu).

Anusha Pokhriyal is with the Department of Physics, University of Illinois at Urbana–Champaign, Urbana, IL 61801 USA (e-mail: pokhriy1@illinois.edu)

Sherine George is with the Department of Bioengineering, University of Illinois at Urbana–Champaign, Urbana, IL 61801 USA (e-mail: sgeorge4@uiuc.edu).

Lu Meng is with SRU Biosystems, Woburn, MA 01801 USA (e-mail: mlu@srubiosystems.com).

vertically emitting mode by first-order diffraction [20]. A schematic cross-sectional diagram of the DFBLB structure is shown in Figure 1(a). The dye doped SU8 layer provides both light confinement along the horizontal direction and amplification of the oscillation mode, while the TiO2 top layer contributes to spatial mode bias into the liquid medium. The DFB laser is optically excited by a frequency doubled, Q-switched Nd:YAG (yttrium aluminum garnet) laser (532 nm, 10 ns pulse width, single pulse mode), and the emission light is coupled into a spectrometer by an optical fiber oriented normal to the device surface. A representative emission spectrum is shown in Figure 1(b). We have previously demonstrated DFBLB devices that were fabricated upon glass and plastic substrates over small surface areas [18, 19], where the dye-doped polymer layer was deposited by spin coating, a process not compatible with roll-to-roll manufacturing. While the dimensions of the replica molded grating structure are highly uniform (as they are determined by the uniformity of the photolithography and etching processes used to create the Si master wafer used for nanoreplica molding), the thickness of the dye-doped polymer layer has been found to determine the uniformity of the both the DFBLB operating wavelength and the device sensitivity. Therefore, we have sought to develop alternative approaches for application of the dye-doped polymer layer, and have adopted a recently demonstrated approach known as "horizontal dipping" [21]. Horizontal dipping is compatible with roll-to-roll mass manufacturing because it is easily controlled, performed at room temperature, and does not require substrate rotation. The process parameters of the horizontal dipping process (blade height, fluid viscosity, dipping speed) can be controlled to accurately produce polymer thin films in the thickness range of ~0.2 - 3.0 μm [21, 22].

In this work, we demonstrate the extension of the nanoreplica molding and horizontal dipping process to large surface areas, enabling the fabrication of 3×5 inch^2 DFBLB active areas that are suitable for incorporation into standard format microplates. We characterize both the short-range and long-range uniformity of the DFBLB operating wavelength, bulk refractive index sensitivity, and biolayer adsorption sensitivity. We also demonstrate the use of the DFBLB microplate for performing an antibody-antigen detection assay, through a dose-response characterization of the cytokine TNF-α. The capabilities demonstrated in this work lay the foundations for the transition of this technology towards roll-to-roll manufacturing, and the ability to produce DFBLB microplates for applications in pharmaceutical screening and protein biomarker diagnostic assays.

II. Methods

A. Design and fabrication of the DFBLB by nanoreplica molding and horizontal dipping

For a second-order DFB laser, the wavelength of the emitted light (λ) is determined by the equation $m\lambda=2n_{eff}\Lambda$, where m represents the diffraction order (m=2 in this case), n_{eff} is the effective refractive index of the guidance layer, and Λ is the period of the structure. n_{eff} is determined by both the index and thickness of guidance layer. Λ is designed to be 400 nm so that the resonance wavelength is within the gain spectrum of the dye. A thin film (~300 nm) of SU-8 (n=1.58) is used as the guidance layer. As the thickness of this film varies, the n_{eff} and the emission wavelength will change correspondingly. Therefore, the standard deviation of the emission wavelength can used to infer the uniformity of the dye-doped SU8 guidance layer. The grating depth is designed to be 40 nm, as discussed in a previous publication [18].

For the nanoreplica molding process, a Si "master" wafer is used as a molding template for producing the DFB grating structure. A single master wafer may be used thousands of times to produce identical gratings. For this work, an 8-inch diameter Si wafer was patterned by nano-imprint lithography using a Molecular Imprints Imprio 50 machine [23, 24], with a 1x1 cm^2 grating imprint template. The nano-imprint lithography process was performed in a step/repeat fashion to create a 9x12 array of individual grating die, with a grating period of Λ=400 nm period, 50% duty cycle on the master wafer. After nano-imprint patterning, the grating structure was permanently transferred into the silicon by reactive ion etching to a depth of 40 nm and subsequent removal of remaining imprint resist by O2 plasma. To prepare the master wafer for replica molding, it was treated with Repel Silane (Amersham Biosciences) for three hours to facilitate mold separation. An SEM photo and AFM measurement (Figure 2(a-b)) confirm that the master wafer conforms to our design specifications.

Following preparation of the master wafer, a replica molding process is used to transfer a negative volume image of the master wafer to a flexible plastic substrate. The process is performed at room temperature, and requires only low mechanical pressure between the mold and the plastic substrate. A small volume (~1mL) of UV curable polymer (PC409, SSCP Co., Ltd.) selected for its low refractive index (n=1.39, at λ=600 nm after curing) was dispensed onto the surface of the master wafer in a thin line pattern (~150×80 mm^2). One edge of a 10×4 cm^2 PET sheet was placed in contact with the polymer, and a ~5 lb teflon-coated aluminum cylinder was rolled over the PET beginning from the edge of the wafer with the line of polymer. As the cylinder rolled over the PET sheet, the polymer trapped between the sheet and the master wafer was squeezed to a thickness of ~1.5 μm, and the trapped air was expelled towards the leading edge of the advancing liquid front. The liquid polymer conformed to the shape of the master wafer, and was cured to a solid by exposure to a high intensity UV lamp (Xenon) for 50s at room temperature. After curing, the replica was peeled away from the master wafer. SEM and AFM were used to measure the dimensions of the resulting structure (Figure 2(c-d)). Finally, the cured polymer was exposed to O_2 plasma for 3 min to render the surface hydrophobic.

Following replica molding, the horizontal dipping process was used to apply the gain layer. Before the dipping process, the active polymer layer was prepared by mixing a 5 mg/ml

solution of Rhodamine 590 dye (Exciton) in CH2Cl2 with SU-8 (5.0 wt %; Microchem) to a volume percentage of 10%. This mixture was sonicated for 1min to improve the homogeneity the solution. The viscosity of the solution was measured to be 1.34 cP.

The horizontal dipping system consists of a custom-built translatable 1mm-diameter cylindrical barrier and a porous vacuum chuck to hold the PET sheet firmly in place. The porous vacuum chuck (Wenesco Inc.) was made of anodized aluminum and machined flat to 0.005 in. tolerance over its 6x4 inch2 area. With the PET/grating sheet held in place, the dipping solution was injected into the gap (1.2 mm) between the barrier and the PET surface. After 1 min., the solution evenly spread to fill the gap, forming a downstream meniscus via capillary force. Next, the barrier was translated smoothly at a speed of 0.1cm/s using a motorized linear translation stage, leaving a thin film of the dye-doped solution on the grating substrate. After the dipping process, the coated device was soft baked on a 95 °C hotplate for 1 min. to remove the solvent. Finally, the film was photopolymerized by exposing to UV radiation (λ = 365 nm lamp source) with exposure dose of 100 mJ cm^{-2}, and subsequently hard baked on a 95 °C hot plate for 2 min. Figure 3(a) shows the device after the horizontal dipping process. The process slightly planarized the grating surface, resulting in periodic surface features of only 1 nm height as measured by AFM (data not shown).

The final fabrication step is deposition of a 10 nm thick layer of TiO_2 over the horizontal-dipped layer using an electron beam evaporator (Denton Vacuum) to improve biomolecular immobilization and sensor sensitivity as demonstrated in previous research [18, 19]. The finished device was trimmed to a 3x5 $inch^2$ "coupon" that was attached with a die-cut pressure-sensitive adhesive sheet to a bottomless 96 well microplate. In the finished device (Figure 3(b)), the 6 mm diameter bottom surface of each microplate well is comprised of a DFBLB biosensor.

B. Detection instrumentation using pulsed laser excitation and spectrometer-based measurement of device laser emission

The detection instrument used in this work has been described in a previous publication [21]. Briefly, the device was optically pumped by a frequency-doubled, Q-switched Nd:YAG pulsed laser (λ=532 nm, 10 ns pulse duration, and maximum repetition rate of 10Hz). The pump source passed through a beam expander and a spatial filter to clean the beam, which was subsequently focused onto a ~4 mm diameter spot on the DFBLB surface by a 10x objective lens. There is no requirement for the device to be illuminated at any specific incident angle, therefore coupling excitation light to the sensor is extremely robust.

The lasing emission was collected by the same 10x objective lens. The collected light passes through a dichroic mirror and a long pass emission filter to eliminate photons at the same wavelength as the pump source. The emission was coupled into a 200 μm diameter optical fiber by a NA=0.25 convex lens to reduce the coupling loss due to the weak confinement in the axis parallel to the grating. The distal end of the fiber was connected to a spectrometer (Horiba, MODEL #550) with a 0.0125 nm resolution between adjacent wavelength data points in the 580 - 600 nm spectral range of the DFBLB. The spectral output of the laser was fitted to a Lorentzian to determine the peak wavelength value (PWV) of the emission with greater resolution than available from the discrete points available from the spectrometer [19].

III. RESULTS

A. Film thickness uniformity measured by laser emission wavelength

Due to the relationship between the lasing wavelength and the guidance layer thickness, the uniformity of the device was investigated by the distribution of the emission wavelength. Figure 4 shows the spatial distribution and histogram of the emission wavelength over the microplate area (5×3 $inch^2$). Measurements were taken at the center of each well and 96 points in total were recorded. The emission wavelengths varied by as much as $\Delta\lambda\approx$9 nm over the whole area, corresponding to ~40 nm thickness variance as determined via Rigorous Coupled Wave Analysis (RCWA) computer simulations of the device structure. As shown in Figure 4, the overall uniformity can be further improved through the use of a larger substrate, since the variation in the thickness near the edges of the sensor coupon is the primary contributor to the total variance. The calculated standard deviation of lasing wavelength was σ=2.35 nm while the mean lasing wavelength was λ_{mean}=568.50 nm, corresponding to a coefficient of variation of CV=0.41%. To characterize the uniformity at a finer spatial scale, 64 points within a single well were also measured. Figure 5 shows the distribution of the lasing wavelength over the ~32 mm^2 area within one well. The emission wavelengths varied by as much as $\Delta\lambda\approx$1.38 nm and the calculated standard deviation was σ=0.40 nm with the mean value λ_{mean}=576.60 nm, corresponding to a CV=0.07%. This corresponds to a thickness variation of the guidance layer of only ~6 nm.

B. Sensitivity uniformity measured by response to adsorption of a protein monolayer

The sensor's bulk sensitivity and uniformity of surface sensitivity were studied by applying liquids with different refractive indices to the sensor surface and measuring the resulting laser PWV shift. To study the device's "bulk" sensitivity, the sensitivity to changes in the refractive index (RI) of media exposed to the sensor surface was measured by placing ~100μL of water (RI=1.33), 35% glycerol (RI=1.37), 55% glycerol (RI=1.41) and 75% glycerol (RI=1.44) in 4 different wells. The recorded laser wavelengths were plotted as function of liquid RI in (data not shown) and a bulk RI sensitivity of $S_b = \Delta\lambda/\Delta n$ was calculated for each well, where Δn is the index change of the medium and $\Delta\lambda$ is the wavelength shift. The average bulk sensitivity over 4 wells was 92.75 nm/RIU, where RIU is the

refractive index unit, and the standard deviation was as small as 0.22 nm/RIU. While the bulk sensitivity measurement is a common metric for optical sensors, probing the device response to surface-based binding is a more useful method to study the performance of the biosensor in the context of a biomolecule binding application. To characterize the near-surface sensitivity, lasing wavelength shifts due to the absorption of a monolayer of protein polymer Poly (Lys, Phe) (PPL, 1mg/mL; Sigma-Aldrich) were measured for 32 wells. The PPL was first dissolved in DI water at concentration of 1mg/mL, and 100µL PPL solution was applied into each well. The PPL monolayer self-assembled on the sensor's surface and stabilized after approximately 10 minutes. Measurements were taken in the center of each well and results are summarized and compared in Figure 6. We observed a PWV shift of 1.01±0.13 nm with CV≈13.60% for the polymeric monolayer. Additionally, in order to characterize the device's short-range uniformity of sensitivity to surface mass absorption, 64 points within one well were also measured and these results are shown in Figure 7. The calculated standard deviation was σ=0.10 nm, the mean value was λ_{mean}=0.84 nm, and the corresponding CV was 11.79%. Detection instrument used in this work has been described in a previous publication [21]. Briefly, the device was optically pumped by a frequency-doubled, Q-switched Nd:YAG pulsed laser (λ=532 nm, 10 ns pulse duration, and maximum repetition rate of 10Hz). The pump source passed through a beam expander and a spatial filter to clean the beam, which was subsequently focused onto a ~4 mm diameter spot on the DFBLB surface by a 10x objective lens. There is no requirement for the device to be illuminated at any specific incident angle, therefore coupling excitation light to the sensor is extremely robust.

C. *Application to an assay for detection of TNF α*

To demonstrate the ability of the sensor to detect biomolecules in the context of a binding assay, four different wells in the sensor microplate were first rinsed and soaked in Phosphate Buffered Saline (PBS) buffer to establish an initial baseline emission wavelength. To functionalize the sensor surface, each well was treated with a 10% solution of polyvinylamine (PVA; provided by SRU Biosystems Inc.) in water and incubated at 40 ºC for 2 hours. All wells were then washed 3 times with water. Each well of the sensor was then exposed to 50 µL glutaraldehyde solution (25% in water; Sigma–Aldrich) for 4 hours, followed by a wash step. Next, a measurement of the emission wavelength from the PBS-immersed laser surface was made and recorded. A 40µL volume of anti-TNF-α (Biolegend; MW=55 kDa) was then pipetted into four wells separately, and allowed to incubate for 30 min at 4C. After rinsing 3x with a solution of PBS with 2% tween (PBST) to remove unbound anti-TNF-α, the emission wavelength from the center spot of each well was measured and wavelength shifts compared to the end point of the previous step were calculated. 40µL of protein-free blocker (Bio-Rad Laboratories) was applied into each well subsequently and allowed to stabilize for 2 hours at room temperature. The spectrum was recorded again as the reference after the surface was washed by PBST. TNF-α (R&D Biosystems Inc.; MW=17 kDa) was dissolved in a 50mL solution of PBS to four different concentrations (5, 2.5, 1.25 and 0.625 µg/mL), and applied separately to each well and stabilized for 30 min. Next, the sensor surface was rinsed with PBST solution to remove any unbound TNF-α. Figure 8 shows the laser wavelength shift end point as a function of TNF-α concentration. For each point, there are 15 data points averaged, which are used to compute the standard deviation. The highest concentration (5µg/mL) of TNF-α detection approaches saturation due to the limited number of anti-TNF-α sites on the sensor surface. The lowest concentration of TNF-α (0.625µg/mL) resulted in the measured laser wavelength shift of ~0.02 nm. As indicated by the inflection point, the dissociation constant K_d was measured to be 1.185µg/mL (0.069 µM), which is comparable with previously measured values of 0.136 µM for human TNF-α and anti-human TNF-α pairs obtained by dual color fluorescence cross correlation spectroscopy [25].

IV. Discussion and Conclusion

The fabrication process described in this work demonstrates, for the first time, the ability to produce DFB biosensor surfaces uniformly over surface areas substantial enough to incorporate into standard format microplates. Although the fabrication was carried out in a laboratory setting, all methods are compatible with extension of the process to a roll-based manufacturing paradigm. In particular, the nanoreplica molding approach used in this work has been implemented upon continuous rolls of plastic film in a step-repeat process that can utilize a master wafer for thousands of iterations without damage [4, 5], while accurately patterning features in the size scale of 40-150 nm. Likewise, the horizontal dipping process used to generate the dye-doped SU_8 layer of the DFBLB has been implemented without the need for spin-coating, while still maintaining excellent control of the layer thickness and uniformity. Incorporation of a label-free sensor into a microplate format represents an important step in the development of a technology that can be accepted into pharmaceutical high throughput screening, as this liquid handling method is heavily utilized for assay automation and integration with standard liquid handling systems. Because the DFBLB grating is semi-continuous, the same sensor format can also be integrated into higher throughput 384-well and 1536-well microplates, which share the same device area as the 96-well microplate demonstrated here. Of course, the DFBLB is not limited to use in a microplate format, as it can also be incorporated into the surface of microscope slides, flasks, tubing, test tubes, or microfluidic channels.

A substantial advantage of the DFBLB sensor surface is that any region on the surface is a sensor, and as a result, capture molecules and illumination can occur at any location. The pump source is not required to enter the device at any particular illumination angle, and only has the requirement of

containing a wavelength that overlaps the excitation spectrum of the DFB laser dye. Therefore, precise coupling conditions are not required, leading to a robust detection platform that is amenable to high throughput measurements. A single 10 ns excitation pulse is sufficient for gathering a measurement, resulting in a rapid detection rate that can be used to gather kinetic information on biomolecular interactions. We also envision a label-free surface scanning detection approach, in which the excitation spot is rastered across the DFBLB surface to generate a spatial map of biomolecular or cellular binding for applications such as label-free microarrays and label-free cell attachment imaging. Our calculations [26] estimate that the liquid volume probed by a single laser pulse can be as small as ~8×10^{-5} pL, assuming that the pumping spot size is near the diffraction limit. All these capabilities are predicated upon the ability to produce DFBLB surfaces that are uniform in terms of the lasing wavelength and the device sensitivity.

ACKNOWLEDGMENT

This project was made possible by a cooperative agreement that was awarded and administered by the National Institutes of Health (Grant R21 EB009695 A), the National Science Foundation (Grant ECCS 09-24062) and the Telemedicine & Advanced Technology Research Center (TATRC), under Contract W81XWH0810701. The authors also extend their gratitude to the support staff of Micro and Nanotechnology Laboratory at University of Illinois at Urbana-Champaign.

REFERENCES

[1] G S. Herminjard, L. Sirigu, H. P. Herzig et al., "Surface Plasmon Resonance sensor showing enhanced sensitivity for CO2 detection in the mid-infrared range," Opt. Express, vol. 17, no. 1, pp. 293-303, 2009.

[2] J. Homola, S. S. Yee, and G. Gauglitz, "Surface plasmon resonance sensors: review," Sensors and Actuators B: Chemical, vol. 54, no. 1-2, pp. 3-15, 1999.

[3] K. Nakatani, S. Sando, and I. Saito, "Scanning of guanine-guanine mismatches in DNA by synthetic ligands using surface plasmon resonance," Nat. Biotechnol., vol. 19, pp. 51-55, 2001.

[4] B. Cunningham, J. Qiu, P. Li et al., "Enhancing the surface sensitivity of colorimetric resonant optical biosensors," Sensors and Actuators B: Chemical, vol. 87, no. 2, pp. 365-370, 2002.

[5] I. D. Block, M. Pineda, C. J. Choi et al., "High Sensitivity Plastic-Substrate Photonic Crystal Biosensor," Sensors Journal, IEEE, vol. 8, no. 9, pp. 1546-1547, 2008.

[6] C. Y. Chao, and L. J. Guo, "Polymer microring resonators for biochemical sensing applications," IEEE J. Selected Topics Quantum Electron., vol. 12, pp. 134-142, 2006.

[7] M. S. Luchansky, and R. C. Bailey, "Silicon Photonic Microring Resonators for Quantitative Cytokine Detection and T-Cell Secretion Analysis," Analytical Chemistry, vol. 82, no. 5, pp. 1975-1981, 2010.

[8] A. J. Qavi, and R. C. Bailey, "Multiplexed Detection and Label-Free Quantitation of MicroRNAs Using Arrays of Silicon Photonic Microring Resonators," Angewandte Chemie International Edition, vol. 49, no. 27, pp. 4608-4611, 2010.

[9] I. M. White, H. Oveys, X. Fan et al., "Integrated multiplexed biosensors based on liquid core optical ring resonators and anti-resonant reflecting optical waveguide," Appl. Phys. Lett., vol. 89, pp. 191106, 2006.

[10] I. M. White, H. Oveys, and X. Fan, "Liquid-core optical ring-resonator sensors," Opt. Lett., vol. 31, no. 9, pp. 1319-1321, 2006.

[11] S. Arnold, "Microspheres, photonic atoms, and the physics of nothing," Am. Sci., vol. 89, pp. 414-421, 2001.

[12] S. Arnold, M. Khoshsima, I. Teraoka et al., "Shift of whispering gallery modes in microspheres by protein adsorption," Opt. Lett., vol. 28, pp. 272-274, 2003.

[13] H. C. Ren, F. Vollmer, S. Arnold et al., "High-Q microsphere biosensor analysis for adsorption of rodlike bacteria," Opt. Express, vol. 25, pp. 17410-17423, 2007.

[14] A. M. Armani, R. P. Kulkarni, S. E. Fraser et al., "Label-free, single-molecule detection with optical microcavities," Science, vol. 317, pp. 783-787, 2007.

[15] A. M. Armani, A. Srinivasan, and K. J. Vahala, "Soft lithographic fabrication of high Q polymer microcavity arrays," Nano Lett., vol. 7, pp. 1823-1826, 2007.

[16] F. Vollmer, and S. Arnold, "Whispering-gallery-mode biosensing: label-free detection down to single molecules," Nat Meth, vol. 5, no. 7, pp. 591-596, 2008.

[17] J.-H. Zhang, T. D. Y. Chung, and K. R. Oldenburg, "A Simple Statistical Parameter for Use in Evaluation and Validation of High Throughput Screening Assays," Journal of Biomolecular Screening, vol. 4, no. 2, pp. 67-73, April 1, 1999, 1999.

[18] M. Lu, S. S. Choi, U. Irfan et al., "Plastic distributed feedback laser biosensor," Applied Physics Letters, vol. 93, no. 11, pp. 111113, 2008.

[19] M. Lu, S. S. Choi, C. J. Wagner et al., "Label free biosensor incorporating a replica-molded, vertically emitting distributed feedback laser," Applied Physics Letters, vol. 92, no. 26, pp. 261502, 2008.

[20] R. Kazarinov, and C. Henry, "Second-order distributed feedback lasers with mode selection provided by first-order radiation losses," Quantum Electronics, IEEE Journal of, vol. 21, no. 2, pp. 144-150, 1985.

[21] C. Ge, M. Lu, X. Jian et al., "Large-area organic distributed feedback laser fabricated by nanoreplica molding and horizontal dipping," Opt. Express, vol. 18, no. 12, pp. 12980-12991, 2010.

[22] B. Park, and M.-y. Han, "Organic light-emitting devices fabricated using a premetered coating process," Opt. Express, vol. 17, no. 24, pp. 21362-21369, 2009.

[23] S. Y. Chou, C. Keimel, and J. Gu, "Ultrafast and direct imprint of nanostructures in silicon," Nature, vol. 417, no. 6891, pp. 835-837, 2002.

[24] S. Y. Chou, P. R. Krauss, and P. J. Renstrom, "Imprint Lithography with 25-Nanometer Resolution," Science, vol. 272, no. 5258, pp. 85-87, April 5, 1996, 1996.

[25] L. Borras, T. Gunde, J. Tietz et al., "Generic Approach for the Generation of Stable Humanized Single-chain Fv Fragments from Rabbit Monoclonal Antibodies," Journal of Biological Chemistry, vol. 285, no. 12, pp. 9054-9066, March 19, 2010, 2010.

[26] C. Ge, "LABEL-FREE BIOSENSOR BASED UPON A VERTICALLY EMITTING DISTRIBUTED FEEDBACK LASER," ECE, UIUC, Urbana, 2010.

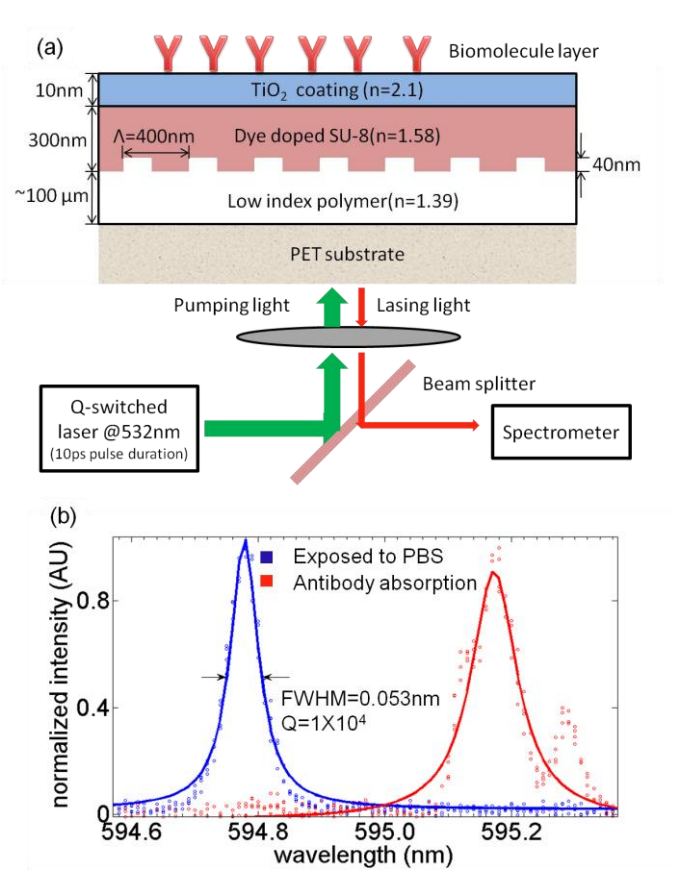

Fig.1. (a) Schematic diagram of the DFBLB structure. The DFB laser is excited by a frequency doubled, Q-switched Nd:YAG laser (532 nm, 10 ns pulse width), and the emission light is coupled into a spectrometer by an optical fiber. (b) Lorentz fitted spectrum of DFB laser emission. The blue curve was measured when the sensor surface exposed to PBS. Full width at half maximum (FWHM) of the lasing emission is 0.053nm, resulting in quality factor=1×10^4 for typical devices reported here. The red curve shows the lasing spectra after application of the anti-TNF-α capture molecules, resulting in a PWV shift of ~0.4nm.

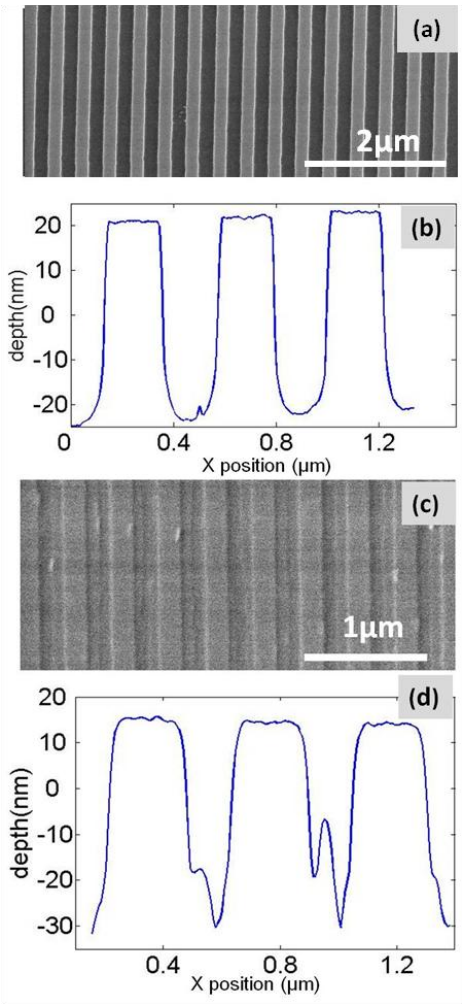

Fig. 2. SEM (a) and AFM (b) images of the master wafer surface, confirming a grating period of Λ=400 nm period, 50% duty cycle on the master wafer. SEM (c) and AFM (d) of the replica molded grating.

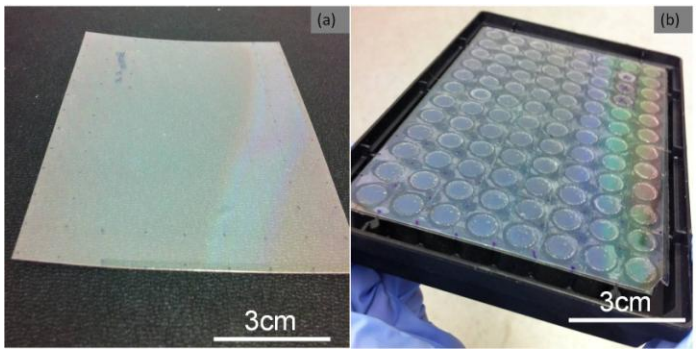

Fig. 3. Photos of DFBLB devices. Before (a) and after (b) the device was bonded to a 96 well bottomless microplate.

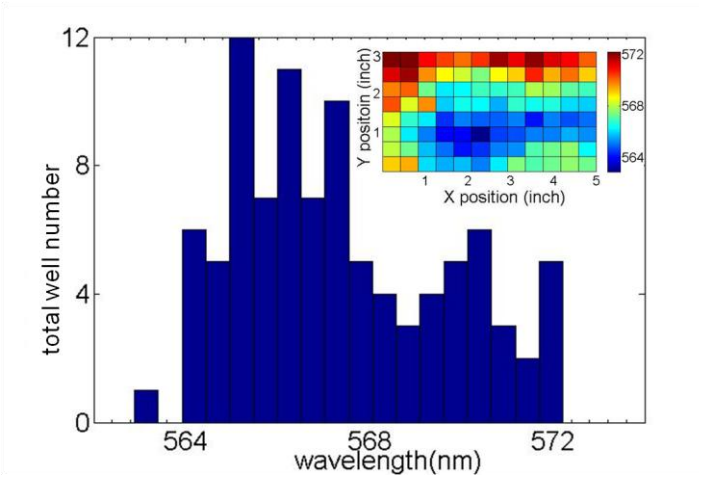

Fig. 4. Histogram of laser emission wavelengths from center region of 96 wells over the DFBLB microplate. The calculated standard deviation was σ=2.35 nm while the mean lasing wavelength was λ_{mean}=568.50 nm, corresponding to a coefficient of variation of CV=0.41%. Inset shows spatial distribution over the device. The color bar represents the emission wavelengths, which varied by as much as $\Delta\lambda\approx$9 nm over the whole area, corresponding to ~40 nm thickness variance.

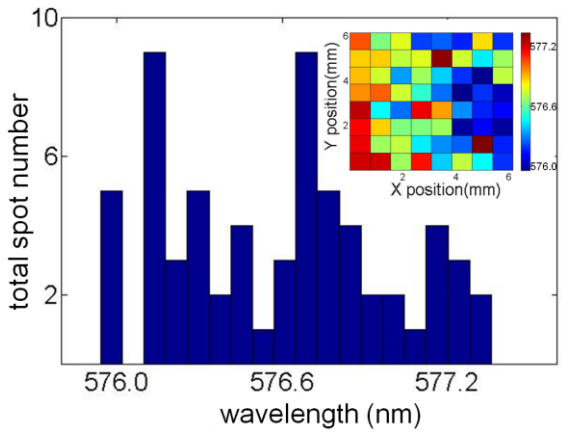

Fig. 5. Histogram of laser emission from 64 points over the 32 mm^2 area within one well of a DFBLB microplate. Inset shows spatial distribution. The emission wavelengths varied by as much as $\Delta\lambda\approx$1.38 nm and the calculated standard deviation was σ=0.40 nm with the mean value λ_{mean} =576.60 nm, corresponding to a CV=0.07% and a thickness variation of the guidance layer of only ~6 nm.

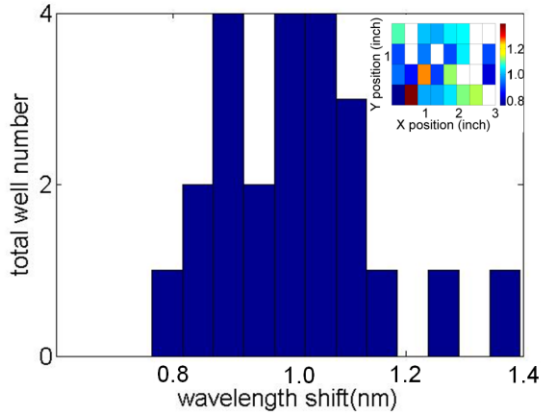

Fig. 6. Histogram of laser wavelength shifts from center of 32 wells due to adsorption of a PPL monolayer. Wavelength shift of 1.01±0.13 nm with CV≈13.60% for the polymeric monolayer was observed. Inset shows the spatial distribution of the wavelength shift for the 32 wells. The blank squares represent locations where the emitted bandwidth had broadened, due to the inhomogeneous binding of the PPL.

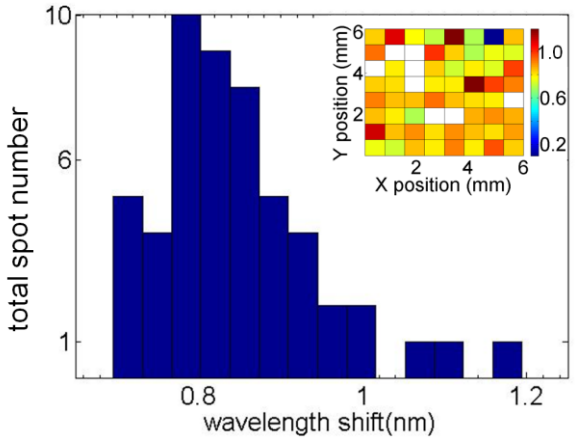

Fig. 7. Histogram of laser wavelength shifts from 64 points within one well due to deposition of a PPL monolayer. The calculated standard deviation was σ=0.10 nm, the mean value was $\Delta\lambda_{mean}$=0.84 nm, and the corresponding CV was 11.79%. Inset shows the spatial distribution of the PPL shift.

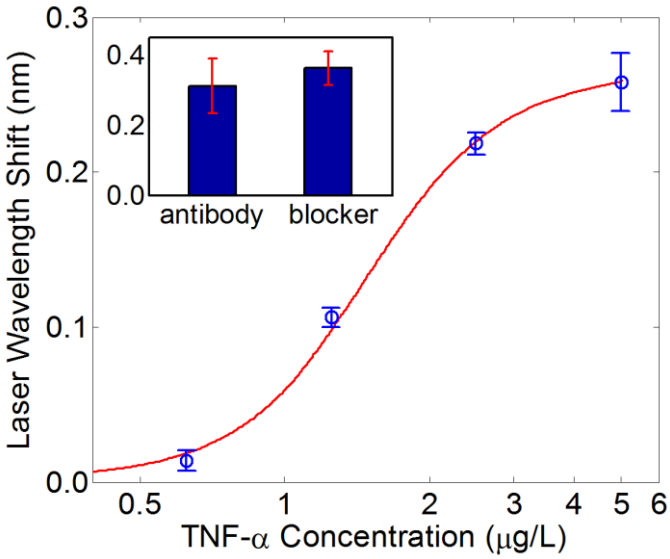

Fig. 8. Laser wavelength shift end point as a function of TNF-α concentration. Inset shows wavelength shift due to surface absorption of anti-TNF-α and protein-free blocker.